

To appear in the Astrophysical Journal

***Chandra* Reveals Variable Multi-Component X-ray Emission from FU Orionis**

Stephen L. Skinner¹, Manuel Güdel², Kevin R. Briggs³, and Sergei A. Lamzin⁴

ABSTRACT

FU Orionis is the prototype of a class of eruptive young stars (“FUors”) characterized by strong optical outbursts. We recently completed an exploratory survey of FUors using *XMM-Newton* to determine their X-ray properties, about which little was previously known. The prototype FU Ori and V1735 Cyg were detected. The X-ray spectrum of FU Ori was found to be unusual, consisting of a cool moderately-absorbed component plus a hotter component viewed through an absorption column density that is an order of magnitude higher. We present here a sensitive (99 ks) follow-up X-ray observation of FU Ori obtained at higher angular resolution with *Chandra* ACIS-S. The unusual multi-component spectrum is confirmed. The hot component is centered on FU Ori and dominates the emission above 2 keV. It is variable (a signature of magnetic activity) and is probably coronal emission originating close to FU Ori’s surface viewed through cool gas in FU Ori’s strong wind or accretion stream. In contrast, the X-ray centroid of the soft emission below 2 keV is offset 0."20 to the southeast of FU Ori, toward the near-IR companion (FU Ori S). This offset amounts to slightly less than half the separation between the two stars. The most likely explanation for the offset is that the companion contributes significantly to the softer X-ray emission below 2 keV (and weakly above 2 keV). The superimposed X-ray contributions from FU Ori and the companion resolve the paradox posed by *XMM-Newton* of an apparently single X-ray source viewed through two different absorption columns.

Subject headings: stars: individual (FU Orionis) — stars: pre-main sequence — X-rays: stars

¹CASA, Univ. of Colorado, Boulder, CO, USA 80309-0389; stephen.skinner@colorado.edu

²Dept. of Astronomy, Univ. of Vienna, Türkenschanzstr. 17, A-1180 Vienna, Austria

³Inst. of Astronomy, ETH Zürich, Wolfgang-Pauli-Str. 27, 8093 Zürich, Switzerland

⁴Sternberg Astronomical Inst., Universitetski Pr. 13, Moscow 119992, Russia

1. Introduction

FU Orionis objects (“FU Ors”) comprise a small class of young stars noted for their powerful optical outbursts. Roughly a dozen known or suspected FUors have been identified, and their properties have been reviewed by Hartmann & Kenyon (1996; hereafter HK96). FUors are undoubtedly young objects in the early phases of stellar evolution. They are found in star-forming regions and are associated with reflection nebulae. Submillimeter observations show that they are surrounded by large quantities of cold dust (Sandell & Weintraub 2001). FUors have strong infrared excesses which can be satisfactorily modeled as accretion disks augmented (in some cases) by cold circumstellar dust. High accretion rates have been inferred from disk models. The optical spectra of FUors are peculiar for young stars and more closely resemble the spectra of F or G supergiants (Herbig 1966; Kravtsova et al. 2007). The unusual spectra are likely dominated by the luminous accretion disk rather than the central star, but interpretations of the complex spectra are controversial (see Petrov & Herbig 1992 for alternative views). Nevertheless, episodic accretion has emerged as the most plausible explanation for their optical outbursts, but the underlying mechanism which initially triggers the accretion event is not yet known. Possible trigger mechanisms are summarized by Reipurth & Aspin (2010).

The prototype FU Orionis increased in visual brightness by ≈ 6 magnitudes during 1936–37 (Herbig 1966). Its brightness has subsequently declined slowly, but has not yet returned to pre-outburst levels. The disk properties of FU Ori have been determined from near-infrared interferometry which gives a disk inclination angle $i \approx 55^\circ$ and a maximum mass accretion rate $\dot{M}_{acc} \sim 10^{-4} M_\odot \text{ yr}^{-1}$ (Malbet et al. 2005; Quanz et al. 2006). Radiative transfer disk models give similar accretion rates (Zhu et al. 2007). The detection of a magnetic field in the disk with a surface strength in the inner disk region of ~ 1 kG has been reported by Donati et al. (2005). Broad P-Cygni absorption profiles show that the accretion is accompanied by strong mass-loss. The estimated mass-loss rate for FU Ori is $\dot{M} \sim 10^{-5} M_\odot \text{ yr}^{-1}$ with a terminal wind speed $v_\infty \approx 250 - 400 \text{ km s}^{-1}$ (Croswell et al. 1987). Despite the high mass-loss rate, the wind is apparently cool as evidenced by the absence of detectable radio continuum emission in a sensitive *VLA* observation (Rodriguez et al. 1990). It has been argued that the wind might arise from the surface of FU Ori’s accretion disk, rather than from the star (Calvet, Hartmann, & Kenyon 1993).

A faint near-IR source (FU Ori S) is located $\approx 0.''5$ south of FU Ori (Wang et al. 2004). High-resolution adaptive optics near-IR observations with the 8 m Subaru Telescope showed the companion to be located at position angle $162.6^\circ \pm 0.4^\circ$ (measured east from north) and separation $0.''493 \pm 0.''003$ from FU Ori (Reipurth & Aspin 2004). At an assumed distance of 460 pc, the projected separation is 227 AU. The companion is 3.9 mag fainter at K' than

FU Ori but has a considerable IR excess and is likely a young K-type star (Reipurth & Aspin 2004).

It has been suggested that the eruptive outbursts characteristic of FUors represent a transient phenomenon experienced in the life of a T Tauri star (TTS). But, the nature of the central star in FUors still remains somewhat of a mystery because of the overwhelming effect of the luminous accretion disk on their optical and near-IR spectra. However, it is known that the FUor V1057 Cyg was a TTS prior to erupting in 1969 (Herbig 1977), giving credibility to the idea that T Tauri stars are the progenitors of some FUors. But, the strong submillimeter emission of FUors also suggests a possible link to class I protostars, as pointed out by Sandell & Weintraub (2001).

Both TTS and class I protostars are routinely detected in X-rays at luminosity levels elevated a thousand-fold above older solar-like main-sequence stars. Because of their youth, one would thus suspect FUors to be luminous X-ray sources. At early evolutionary stages, X-rays could be produced by magnetic activity or in shocks associated with their strong accretion or winds. Until recently, the X-ray properties of FUors were largely unknown. We have thus undertaken an exploratory X-ray survey of FUors using *XMM-Newton*. Of the four classical FUors observed, two were detected: the prototype FU Ori ($\log L_X = 30.8 \pm 0.4$ ergs s⁻¹; Skinner et al. 2006; hereafter S06) and V1735 Cyg ($\log L_X = 31.0 \pm 0.2$ ergs s⁻¹; Skinner et al. 2009). These unabsorbed X-ray luminosities are at the high end of the range found for T Tauri stars. In contrast, the FUors V1057 Cyg and V1515 Cyg were undetected at upper limits $\log L_X \leq 30.0$ and 30.5 ergs s⁻¹ (Skinner et al. 2009). More sensitive observations of these two stars are needed to determine if faint emission is present.

The CCD X-ray spectrum of FU Ori obtained with *XMM-Newton* was based on ≈ 27 ks of low-background EPIC pn exposure and is quite unusual (Fig. 2 of S06). It consists of a cool plasma component at $kT_{cool} \approx 0.65$ keV viewed under moderate absorption, and a much hotter component at $kT_{hot} \gtrsim 4$ keV whose absorption column density is at least ten times larger ($N_H \sim 10^{23}$ cm⁻²). By comparison, the *XMM-Newton* spectrum of the only other detected FUor V1735 Cyg could be reproduced with a simpler one-temperature model consisting of a very hot plasma component at $kT_{hot} \geq 6.4$ keV, also viewed through high absorption $N_H \approx 10^{22.8}$ cm⁻² (Skinner et al. 2009). The existence of two unequal absorption columns in FU Ori’s spectrum is a clue that the cool and hot plasma components originate in spatially distinct regions. Interestingly, similar X-ray spectra with two absorption components have been found for a few jet-driving TTS (Güdel et al. 2007). The most spectacular example is DG Tau, which shows soft low-absorption X-ray emission offset from the star and extending outward $\approx 5''$ along the optical jet and counterjet axes, plus hard high-absorption emission from the central star (Güdel et al. 2005, 2008; Schneider & Schmitt 2008). These

jet-driving TTS are discussed further in Section 4.5.

XMM-Newton lacked sufficient angular resolution to distinguish between FU Ori itself and the faint IR companion lying $0.''5$ to the south, raising the possibility that the unusual X-ray spectrum might be the superimposed emission of two closely-spaced objects. We present here a deeper 99 ks follow-up observation of FU Ori obtained at higher angular resolution with *Chandra*. Our primary objective was to utilize *Chandra*’s sharp PSF to determine whether the X-ray emission peak is coincident with FU Ori, or if a sub-arcsecond southward offset is present - as could be the case if the near-IR companion is contributing to the X-rays. We show that the hard emission (>2 keV) is dominated by FU Ori itself, and is variable. In contrast, the soft emission (<2 keV) is non-variable and its peak is offset slightly to the southeast of FU Ori, toward FU Ori S. We discuss possible explanations for the offset, the most likely of which is that the companion is an X-ray emitter.

2. Chandra Observations

The *Chandra* observation (ObsId 9924) began on 2008 November 24 at 02:43 TT and ended on November 25 at 09:20 TT. The exposure live time was 98,867 s. Exposures were obtained using the ACIS-S (Advanced CCD Imaging Spectrometer) array in faint timed-event mode with 3.2 s frame times. FU Ori was placed at the nominal aimpoint on the ACIS-S3 CCD. For an on-axis point source, the ACIS-S 70% encircled energy radius at 2 keV is $R_{70} \approx 1.''17$ and the 90% encircled energy radius at 2 keV is $R_{90} \approx 1.''96$ ⁵. For the energy range considered here (0.3 - 8 keV), R_{70} is nearly independent of energy but R_{90} increases slightly with energy. The on-axis absolute astrometric positional accuracy of *Chandra* ACIS-S is $\approx 0.42''$. More information on *Chandra* and its instrumentation can be found in the *Chandra* Proposer’s Observatory Guide (POG)⁶.

The Level 2 events file provided by the *Chandra* X-ray Center (CXC) was analyzed using standard science threads in CIAO version 4.1.2⁷. The CIAO processing used calibration data from CALDB version 4.1.2. Source detection was carried out using the CIAO *wavdetect* tool, which correlates the input image with “Mexican Hat” wavelet functions of different scale sizes. We ran *wavdetect* on full-resolution images with a pixel size of $0.''492$ using

⁵http://cxc.harvard.edu/cal/Acis/Cal_prods/psf/eeer_on.html

⁶See <http://asc.harvard.edu/proposer/POG>

⁷Further information on *Chandra* Interactive Analysis of Observations (CIAO) software can be found at <http://asc.harvard.edu/ciao>.

events in the 0.3 - 8 keV range to reduce the background. The *wavdetect* threshold was set at $sigrthresh = 1.5 \times 10^{-5}$ and scale sizes of 1, 2, 4, 8, and 16 were used. The *wavdetect* tool provides source positions and net source counts (background-subtracted and PSF-corrected) inside the computed 3σ source region (Table 1).

CIAO *specextract* was used to extract source and background spectra along with source-specific response matrix files (RMFs) and auxiliary response files (ARFs). We used the 3σ source ellipse from *wavdetect* to define the source spectrum extraction region and the background spectrum was extracted from adjacent source-free regions. Background is negligible, contributing <4 counts (0.3 - 8 keV) inside the source extraction region over the duration of the observation. This amounts to $<1.4\%$ of the total counts within the 3σ source ellipse.

Spectral fitting and image analysis were undertaken with the HEASOFT *Xanadu*⁸ software package including XSPEC vers. 12.4.0 and XIMAGE vers. 4.4. X-ray light curves were extracted from the 3σ source ellipse region using the CIAO tool *dmextract*. Checks for source variability were carried out on energy-filtered source event files using the Kolmogorov-Smirnov (KS) test (Press et al. 1992) and the Bayesian-method CIAO tool *glvary* (Gregory & Loredó 1992, 1996).

3. Results

3.1. Image Analysis and Source Identification

Table 1 summarizes the basic X-ray properties of FU Ori. Our image analysis addressed three questions: (i) is the broad-band X-ray centroid coincident with the position of FU Ori, to within *Chandra* positional accuracy, (ii) is there any significant offset between the X-ray positions of the soft and hard X-ray components of FU Ori, and (iii) is the X-ray source associated with FU Ori a point source at *Chandra*'s spatial resolution? The presence of any offset or extension toward the south would be a clue that the companion is contributing to the X-ray emission.

To measure X-ray positions, we first removed the pixel randomization which is applied by default during the *Chandra* ACIS standard processing. Energy filters were then applied to the de-randomized event files in three bands: broad (0.3 - 8 keV), soft (0.3 - 2 keV), and hard (2 - 8 keV). Energy-filtered images were then created in each band using the physical pixel size (0."492) and smaller subpixel sizes of 0."25 and 0."125. X-ray centroids were

⁸<http://heasarc.gsfc.nasa.gov/docs/xanadu/xanadu.html>.

then measured in the subpixel images using the *centroid* task in XIMAGE⁹. Pixels inside a square box of size $2.''4 \times 2.''4$ (box half-width = $1.''2$) centered on the source were used for the centroid measurements. This box half-width equals the 70% encircled energy fraction and captures essentially all source photons (Fig. 1). Centroid positions from XIMAGE were compared with those obtained using the CIAO *dmstat* tool and were found to be in excellent agreement.

The measured X-ray centroid of the source identified as FU Ori in the broad-band image was found to be (J2000.0): R.A. = $05^h 45^m 22.385s$, Decl. = $+09^\circ 04' 12.40''$. This position is offset by $(\Delta\text{R.A.}, \Delta\text{Decl.}) = (+0.028s, 0.''00)$ from the 2MASS near-IR position of FU Ori: 2MASS J054522.357+090412.40. The above offsets are in the sense of CXO – 2MASS. Thus, the X-ray position determined from *Chandra* standard processing has a r.m.s. offset of only $0.''41$ from FU Ori, which is just within *Chandra*'s ACIS-S absolute astrometric accuracy of $\approx 0.''42$ (90% confidence) for near on-axis sources¹⁰.

To fine-tune the *Chandra* positional registration relative to 2MASS, we identified two other X-ray sources near FU Ori on the same CCD (chip S3) which had 2MASS counterparts: 2MASS J054521.540+090545.71 and 2MASS J054519.296+090322.61. These were the only two sources in the X-ray image with 2MASS counterparts near FU Ori that were bright enough to yield reliable X-ray positions. Our broad-band X-ray centroid measurements of these two sources gave respective offsets relative to 2MASS of $(\Delta\text{R.A.}, \Delta\text{Decl.}) = (+0.025s, +0.''09)$ and $(+0.019s, +0.''11)$. Combining the offsets of these two sources with that of FU Ori gives a mean offset of $(\Delta\text{R.A.}, \Delta\text{Decl.})_{\text{mean}} = (+0.024s, +0.''07)$, in the sense of CXO – 2MASS. Applying this mean offset to the broad-band X-ray position of FU Ori above from the standard processing gives the corrected J2000.0 centroid position (Table 2) R.A._(corr) = $05^h 45^m 22.361s$, Decl._(corr) = $+09^\circ 04' 12.33''$. This corrected position is in excellent agreement with the 2MASS position of FU Ori, with a r.m.s. offset of just $\Delta P = 0.''09$. There is thus no doubt that the X-ray emission detected by *Chandra* is dominated by FU Ori.

We then compared the X-ray centroid of FU Ori measured in subpixel soft-band (0.3 - 2 keV) and hard-band (2 - 8 keV) images. Unsmoothed and smoothed versions of these images are shown in Figure 1. A histogram representation of the distribution of soft and hard counts in the N-S direction within the 70% enclosed energy circle is shown in Figure 2. After applying the mean offsets determined above to the measured soft and hard-band X-ray centroid positions, the hard-band centroid is in very good agreement with the broad-band

⁹<http://heasarc.gsfc.nasa.gov/docs/xanadu/ximage/ximage.html>

¹⁰<http://cxc.harvard.edu/cal/ASPECT/celmon/>

and 2MASS positions (Table 2). The corrected hard-band position is offset by only $0.''04$ from the 2MASS position of FU Ori. The hard-band emission is clearly centered on FU Ori, but the distribution of hard counts shows a slight asymmetry with an excess $\approx 0.''5 - 0.''7$ to the south of FU Ori (Fig. 2-right). The two-component Gaussian fit in Figure 2-right attributes 27 [4 - 48; 90% conf.] counts to the companion, which equates to 12% of the total number of hard counts. Thus, the companion seems to be contributing weakly to the hard emission. But FU Ori is undoubtedly the dominant hard X-ray emitter in the system.

In contrast, the soft-band X-ray centroid is offset slightly to the southeast of FU Ori. Specifically, the displacement of the soft-band X-ray centroid relative to FU Ori’s 2MASS position is 0.006 s ($= 0.''09$) eastward and $0.''18$ southward (Table 2). The r.m.s positional offset of $0.''20$ is small, amounting to slightly less than one-half the $0.''492$ ACIS physical pixel size, but is nevertheless quite apparent in the smoothed subpixel soft-band image in Figure 1. The offset of the soft X-ray centroid relative to FU Ori’s 2MASS position is along P.A. = 154° , which is in the general direction of the companion at P.A. = 162.6° (Reipurth & Aspin 2004). This is a strong indication that the companion is contributing to the soft X-ray emission. A quantitative estimate of the companion’s contribution to the soft-band emission comes from the two-component Gaussian model shown in Figure 2-left. This model attributes about half of the soft-band counts to the companion, but there is considerable leeway on how the soft-band counts can be apportioned between the two stars when 90% confidence ranges are considered.

Some further consideration of whether the soft-band centroid offset might be an observational or statistical artifact is warranted. Several factors suggest that it is not. First, the offset is still present when the subpixel images are reanalyzed with the default pixel randomization retained. Second, the $0.''16$ southeastward offset of the soft X-ray peak relative to the hard peak in FU Ori is much larger than for other nearby X-ray sources. We compared the soft and hard band offsets of three sources near FU Ori on the same CCD (chip S3), namely J054516.93+090545.7 ($1.3'$ off-axis), J054516.93+090502.6 ($1.4'$ off-axis), and J054514.84+090256.9 ($2.4'$ off-axis). Their soft–hard centroid position offsets were $0.''10$, $0.''09$, and $0.''08$, respectively. In declination, the respective offsets were $+0.''05$, $-0.''03$, and $-0.''03$. By comparison, the soft–hard offset of $0.''15$ in declination for FU Ori is $\approx 3 - 5$ times larger, clearly making FU Ori an unusual case. Third, the probability of obtaining a soft-band offset of $0.''20$ relative to the 2MASS position of FU Ori after cross-registration is very low. The statistical uncertainty in the X-ray centroid for near on-axis point sources is primarily determined by the number of source counts. For FU Ori, we obtained 59 soft-band counts and 223 hard-band counts yielding 282 total counts (source+background). This total is slightly less than the value given in Table 1, which is corrected for PSF effects. *Chan-*

dra calibration studies ¹¹ show that the statistical uncertainty in the soft-band centroid is expected to be $<0.''2$ (90% confidence), with negligible uncertainty in the higher-count hard-band centroid measurement. The above considerations leave little doubt that the soft-band centroid offset of $0.''20$ observed for FU Ori is a real physical effect.

As a final check, we used the CIAO tool *srcextent* to determine if FU Ori’s emission is extended. No event filtering on energy was applied in the *srcextent* analysis. Before running *srcextent*, we created a custom point-spread-function (PSF) file for our observation using the *Chart* and *MARX* simulators, as prescribed in the standard CIAO science threads. Using this PSF file, *srcextent* yields an observed source size for FU Ori of $0.''50$ [$0.''45$ - $0.''54$; 90% confidence range], an intrinsic source size of $0.''06$ [$0.''00$ - $0.''50$], and a PSF size of $0.''49$ [$0.''44$ - $0.''54$] ¹². The above analysis shows that despite the small subpixel offset between the soft and hard X-ray centroids, the overall source structure is still compatible with point-like emission at *Chandra*’s resolution. Although modest extension on an angular scale of $\approx 0.''50$ is allowed when 90% confidence ranges are considered, there is certainly no evidence for an X-ray jet in FU Ori extending outward several arcseconds from the star like that found in DG Tau. As Figure 1 shows, essentially all of the detected emission lies within the 70% encircled energy radius.

In summary, we conclude that the hard X-ray emission detected by *Chandra* peaks at the position of FU Ori, and FU Ori is the dominant hard X-ray source in the system. But, a weak hard-band contribution from the companion seems to be present. In contrast, the soft X-ray emission peak is not strictly coincident with FU Ori, but is displaced by $\approx 0.''20$ toward the southeast, amounting to slightly less than half the distance between FU Ori and the companion. Gaussian fits attribute about half of the counts below 2 keV to the companion, indicating that it is contributing significantly to (but may not be entirely responsible for) the soft-band emission.

3.2. X-ray Variability

Both the KS test and *glvary* give a high probability of variability. As Figure 3 shows, the hard emission (2 - 8 keV) is variable but the soft emission (0.3 - 2 keV) is steady. This is a new result, as no significant variability was detected in the shorter ≈ 30 ksec *XMM-Newton* exposure. The hardness ratio, or ratio H/S of hard to soft counts, is also variable. During

¹¹http://cxc.harvard.edu/cal/ASPECT/improve_astrometry.html

¹²Further information on how source sizes are determined by *srcextent* can be found at: <http://cxc.harvard.edu/ciao/ahelp/srcextent.html>.

the first half of the observation we obtained $H/S = 2.8$ and during the second half $H/S = 4.4$. The increase in hardness was accompanied by a temperature increase (Sec. 3.3). Further implications of the variability are discussed in Section 4.2.

3.3. The X-ray Spectrum of FU Ori

Figure 4 shows the ACIS-S CCD spectrum of FU Ori overlaid on the previous *XMM-Newton* EPIC pn spectrum. Overall, the two spectra are similar, consisting of softer emission below 2 keV plus a harder component extending up to ≈ 7 keV. Both spectra clearly show the Fe K emission line complex (Fe XXV) at 6.67 keV, which has maximum line power at $T \sim 40$ MK and is a signature of very hot plasma. The Fe K line flux from ACIS-S is $F_{X,Fe-K} = 1.1 (1.3) \times 10^{-14}$ ergs cm $^{-2}$ s $^{-1}$, where the value in parentheses is unabsorbed. There is no clear ACIS-S detection of fluorescent neutral or near-neutral Fe line emission at 6.4 keV and we obtain an upper limit on the absorbed line flux $F_{X,Fe(6.4)} \leq 2.6 \times 10^{-15}$ ergs cm $^{-2}$ s $^{-1}$ (1σ). The line-like features in the *XMM-Newton* EPIC pn spectrum near 2.46 keV and 2.9 keV may be due to S XV, but these are not visible in the *Chandra* spectrum. Thus, the only unambiguous line detection in the *Chandra* spectrum is the Fe K complex at 6.67 keV.

We have attempted to fit the *Chandra* spectrum with several different emission models, as discussed below. Acceptable fits with multi-temperature thermal plasma models require at least two different absorption components (N_H), as summarized in Table 3. A similar conclusion was reached on the basis of *XMM-Newton* spectral fits (S06).

The simplest model that provides a reasonably good fit to the ACIS-S spectrum assumes two separate isothermal plasma components, each viewed through a different absorption column and represented in notational form as: $N_{H,1} \cdot kT_1 + N_{H,2} \cdot kT_2$ (model A in Table 3). This model and the others in Table 3 are based on the *apec* optically thin thermal plasma model in XSPEC. The absorption column density determined for the hot component ($N_{H,2}$) is about ten times larger than for the cool component ($N_{H,1}$) and the hot component dominates the emission measure (EM) and unabsorbed flux. The N_H and kT values inferred from model A agree with those obtained from a similar fit of the EPIC pn spectrum (Table 1 of S06), to within 90% confidence limits.

The spectral fit can be improved by adding more model components. If the emission is the superposition of a high-absorption contribution from FU Ori and a lower absorption contribution from the companion (Sec. 4), then the assumption in model A that each component is isothermal is overly simplistic. T Tauri star X-ray spectra generally show both cool and hot plasma components, indicative of coronal plasma distributed over a range of

temperatures (Preibisch et al. 2005). Thus, some fit improvement might be obtained by replacing each of the isothermal components in model A with a two-temperature plasma; that is: $N_{H,1} \cdot kT_1 \rightarrow N_{H,1} \cdot (kT_{1,cool} + kT_{1,hot})$ for the low-absorption component and similarly $N_{H,2} \cdot kT_2 \rightarrow N_{H,2} \cdot (kT_{2,cool} + kT_{2,hot})$ for the high-absorption component. In order to achieve a stable fit, we considered a slightly simplified form of the above model. Specifically, for the low-absorption component which dominates the emission below 2 keV but has relatively few detected counts, we adopted a fixed value $kT_{1,hot} = 3$ keV, typical of coronal sources. For the high-absorption component which dominates the emission above 2 keV, we ignored the $kT_{2,cool}$ contribution since any cool plasma produced in FU Ori is almost entirely absorbed and its spectral properties are not constrained by the *Chandra* data. The above simplifications reduce the number of free plasma temperature components in the model from four to two. The fit results are summarized in model B of Table 3. As can be seen, this model results in a significant reduction in the χ^2 fit statistic compared to model A, largely because of an improved fit to the spectrum below 2 keV (Fig. 5). This is a good indication that the low-absorption component is not isothermal.

We also consider a third model consisting of three unequal absorption components, each associated with an isothermal plasma (model C). This model may be justified on physical grounds if there is a third star in the system, as suggested by several previous studies (Malbet et al. 2005; Vittone & Errico 2005; Reipurth & Aspin 2004). This model provides a near-perfect fit below 2 keV (Fig. 5) but the reduced χ^2 value is identical to that of model B. Although the fit below 2 keV is excellent, the temperature of the coolest component in model C overlaps that of the intermediate temperature component when 90% confidence ranges are considered (Table 3). Thus, the physical distinction between the cool and intermediate temperature components is somewhat ambiguous.

In the above models, essentially all of the detected emission above 2 keV is due to the heavily-absorbed hot component from FU Ori, as shown in the unfolded spectra in Figure 6. Models A and B place >90% of the emission measure in the hottest component, while model C attributes 71% to the hottest component. Based on unabsorbed flux measurements (Table 3), the spectral models give unabsorbed X-ray luminosities for FU Ori of $\log L_X(0.3 - 8 \text{ keV}) = 30.76 - 31.09 \text{ ergs s}^{-1}$. The correction for absorption is quite large, as can be seen by comparing the absorbed and unabsorbed fluxes in Table 3. Nevertheless, the unabsorbed *Chandra* fluxes and luminosities are similar to those determined from *XMM-Newton* (S06). The high-temperature component arising in FU Ori accounts for $\geq 90\%$ of the intrinsic X-ray luminosity in models A and B, and 65% in model C. The X-ray luminosity of FU Ori is at the high end of the range compared to accreting TTS, as discussed further in Section 4.4

When fitting the *XMM-Newton* EPIC pn spectrum, a significant improvement in the

goodness-of-fit (reduced χ^2) was obtained by replacing the high-temperature thermal plasma component with a power-law model plus a Gaussian Fe K line at 6.67 keV (S06). We repeated this procedure when fitting the *Chandra* ACIS-S spectrum. We found essentially no change in the reduced χ^2 values when the high-temperature thermal component in the models in Table 3 was replaced by a power-law plus Gaussian line. Thus, the *Chandra* data show no clear preference for a nonthermal interpretation of the hard X-ray component.

We have compared the X-ray spectrum of FU Ori during the first and second half of the observation. Spectral fits with the 3T *apec* model show that the observed (absorbed) X-ray flux (0.3 - 8 keV) in the first half was $F_X = 4.8 \times 10^{-14}$ ergs cm $^{-2}$ s $^{-1}$, increasing to 7.8×10^{-14} ergs cm $^{-2}$ s $^{-1}$ in the second half. The spectrum hardened in the second half (Sec. 3.2) and the temperature of the hot component increased to $kT_{hot} \approx 5.4$ keV in the second half compared to $kT_{hot} \approx 2.2$ keV in the first half. There are insufficient counts in the time-partitioned spectra to determine whether any spectral variability occurred in the cool component. But, any significant spectral changes seem unlikely given that no time-variability was detected in the soft-band.

4. Discussion

We discuss physical processes that might be responsible for the soft and hard X-ray components in FU Ori below. We also elaborate on FU Ori’s high X-ray absorption, high X-ray luminosity, and draw comparisons with jet-driving TTS.

4.1. The Soft X-ray Component

The 0."2 southeastward offset of the soft X-ray peak from FU Ori equates to a projected linear separation of ~ 92 AU at $d = 460$ pc. Although some soft emission might penetrate FU Ori’s high absorption, as discussed below, no positional offset would be expected if the soft emission detected by *Chandra* originated *entirely* near FU Ori’s surface (e.g. in a cool coronal component, or an accretion shock). To account for the offset, an additional contribution that is not coincident with FU Ori must be present.

Possible scenarios that could produce soft emission offset slightly from FU Ori include the following: (i) a one-sided X-ray microjet, (ii) scattering into the line-of-sight of soft X-rays which manage to escape from near the star through an outflow cavity, (iii) shock

emission formed as FU Ori’s wind collides with either the wind of the companion or dense material between the two stars, and (iv) a soft X-ray contribution from the companion itself. Any plausible explanation must account for the fact that the soft emission is offset toward the companion, and we thus regard the last explanation as the most likely.

We are not aware of any reports of an optical jet from FU Ori that is directed southeast toward the companion, but work in progress suggests that a collimated outflow directed toward the northeast may be present (see below). In any case, a chance alignment of any jet toward the companion would be quite unusual. Since X-ray jets trace optical jets (e.g. DG Tau), the one-sided jet interpretation has little observational support so far.

Scattering of X-rays by infalling or outflowing material was proposed as one means of explaining the small $\approx 0.''5 - 1.''0$ offset of the *Chandra* X-ray position from the L1551-IRS 5 binary protostar (Bally, Feigelson, & Reipurth 2003). L1551-IRS 5 drives a Herbig-Haro jet (HH 154) and is similar to FU Ori in that the absorption directly toward the central source IRS 5 is very high ($N_H \approx 10^{23.5} \text{ cm}^{-2}$). Direct escape of soft X-rays is blocked but they could escape indirectly through the HH 154 outflow cavity and then be reflected by dense material into the line-of-sight (Fig. 5 of Bally et al. 2003). Work in progress also reveals a HH object $\approx 2''$ northeast of FU Ori (P. Garcia et al., in prep.), but no X-ray emission was detected by *Chandra* at the HH object position (P. Garcia, priv. comm.). If FU Ori is the driving source then this HH object could create an outflow cavity for soft X-rays to escape. However, the emergence of any such reflected X-rays in a direction toward the companion would be quite fortuitous, making this interpretation difficult to justify for FU Ori.

The production of soft X-rays from a shock formed as FU Ori’s strong wind collides with the companion’s wind or other dense intervening material deserves consideration. The hottest shocked plasma in such a colliding wind system is expected to form on the line-of-centers between the two stars, consistent with the observed offset direction. Furthermore, the kinetic energy in FU Ori’s wind is more than adequate to account for the X-ray luminosity of the soft component. Assuming $\dot{M} \sim 10^{-5} M_\odot \text{ yr}^{-1}$ and $v_\infty \approx 250 - 400 \text{ km s}^{-1}$, FU Ori’s wind luminosity $L_{wind} = (1/2)\dot{M}v_\infty^2$ is $\log L_{wind} = 35.3 - 35.7 \text{ ergs s}^{-1}$. This is more than 5 orders of magnitude greater than the X-ray luminosity of the cool component. However, closer inspection reveals difficulties with the wind-shock interpretation. First, if the companion is physically associated with FU Ori then its orbit should be nearly coplanar with FU Ori’s disk plane. In that case, FU Ori’s disk would tend to shield the companion if FU Ori’s wind is stellar. If FU Ori has a disk wind then it would flow outward at some angle from the disk (Fig. 1 of Calvet et al. 1993). In that case, only a fraction of the wind’s total velocity vector would be directed toward the companion, and such a geometry is not favorable for strong wind-shock emission. Second, for a wind of speed v shocking onto a stationary target,

the predicted shock temperature is $T_s = 1.5 \times 10^5 (v/100 \text{ km s}^{-1})^2 \text{ K}$ (Raga et al. 2002). Setting v equal to FU Ori’s terminal wind speed $v_\infty \approx 250 - 400 \text{ km s}^{-1}$ (Croswell et al. 1987; Herbig, Petrov, & Duemmler 2003), the above relation gives $T_s \approx 0.94 - 2.4 \text{ MK}$, or $kT \approx 0.1 - 0.2 \text{ keV}$. With the possible exception of the coolest component in models B and C, these temperatures are too low to account for those inferred from the X-ray fits (Table 3). Higher temperatures could be achieved if FU Ori’s wind were shocking onto a high-speed wind or outflow from the companion (as opposed to a stationary target), but specific information on the companion’s mass-loss rate and wind/outflow speeds is not available. Until such data are obtained, more detailed comparisons with wind shock model predictions cannot be made. The wind parameters of the companion are important because the location of the shock contact discontinuity on the line-of-centers between the two stars where the maximum shock temperature occurs is determined by the ratio of FU Ori’s wind momentum ($\dot{M}v_\infty$) to that of the companion (eq. [1] of Stevens, Blondin, & Pollock 1992). In order to place the discontinuity near the midpoint between the two stars where the soft X-ray peak is located, the wind momenta of the two stars would need to be nearly equal. This would require a very strong companion wind, which is unlikely if the companion is a K-type TTS because their mass-loss rates are typically much less than that of FU Ori (Hartigan, Edwards, & Ghandour 1995).

The final possibility is that the companion is an intrinsic X-ray source and emits some of its radiation below 2 keV. This seems quite likely because K-type pre-main sequence stars (TTS) are commonly detected as X-ray sources, and we have already noted that the companion is probably contributing weakly to the harder emission above 2 keV (Fig. 2-right). A cool plasma component would also be expected since spectral fits of TTS in the Orion COUP sample typically required two-temperature models with cool-component temperatures of $kT_{cool} = 0.2 - 0.9 \text{ keV}$, most of which lie at the high end of this range (Preibisch et al. 2005). The nearly ubiquitous presence of this cool plasma suggests that it is coronal (Preibisch et al. 2005). In order to shift the soft-band centroid to a position between the two stars (as observed), a soft-band contribution from FU Ori would also be required. That is, the emission below 2 keV would be interpreted as the superimposed contribution of soft photons from FU Ori and the companion. Despite the high absorption toward FU Ori, it is likely that some soft $E < 2 \text{ keV}$ photons do escape. As Figure 2-left shows, the soft-band counts at FU Ori’s position are not zero. XSPEC simulations show that if FU Ori has a cool plasma component at $kT_{cool} \approx 0.2 - 0.9 \text{ keV}$ and hotter plasma at $kT_{hot} \approx 3 - 4 \text{ keV}$ (as typical for young low-mass stars in Orion) and is viewed through homogeneous absorption $N_H \sim 10^{23} \text{ cm}^{-2}$, then up to several percent of the emergent photons can have energies $E < 2 \text{ keV}$. However, the XSPEC simulations do not take into account factors that could increase the escape probability for soft photons such as inhomogeneous

absorption or incomplete occultation of the corona by the disk (Fig. 6 of Kravtsova et al. 2007). The best-fit two-component Gaussian model of the soft-band count distribution in the N-S direction (Fig. 2-left) apportions the 59 soft-band counts roughly equally between FU Ori with 28 [14 - 40] counts and the companion with 31 [16 - 42] counts, where brackets enclose 90% confidence intervals. As the confidence ranges show, the superposition model is acceptable even with as few as 14 counts attributed to FU Ori. At the high end of the 90% confidence range, FU Ori could be responsible for the majority of soft-band photons, but not all of them. Indeed, if all of the soft photons were attributed to FU Ori then the means by which they managed to escape through FU Ori’s high absorption would have to be explained and the need for a spectral model with multiple absorption components would be much less obvious.

4.2. The Hard X-ray Component

The hot component has a plasma temperature $kT_{hot} \approx 3 - 4$ keV (and $kT_{hot} > 5$ keV during the flare) which is characteristic of coronal sources. The long *Chandra* exposure shows that the hard emission associated with FU Ori is variable, as is commonly the case in magnetically-active young stars.

The most straightforward explanation of the hot plasma is that it originates in a magnetically-active corona. A more speculative possibility is that the hard X-rays originate in the magnetic interconnection region between the star and inner disk, or in the disk itself. The observations of Donati et al. (2005) provide evidence that the disk is magnetized and the the field is filamentary and reaches strengths of ~ 1 kG toward the disk center. Could such an environment lead to X-ray production via a disk corona? Distinguishing between X-ray production in a stellar corona or in the disk corona or star-disk interaction region will be difficult because of spatial resolution limits of current X-ray telescopes. Models based on VLTI interferometry give an inner disk radius for FU Ori of $R_{in} \approx 5 R_{\odot}$ (Malbet et al. 2005; Quanz et al. 2006). This radius corresponds to an angular size of 0.05 mas at $d = 460$ pc.

The rise and fall of the hard-band count rate spanned less than one day. Exponential fits of the hard-band light curve give a rise time $\tau_{rise} \sim 45$ ks ($= 0.52$ d) and $\tau_{decay} \sim 23$ ks ($= 0.27$ d). By comparison, estimates of FU Ori’s rotation period are in the range 8.8 d (Popham et al. 1996; see also Errico, Vittone, & Lamzin 2003) to 14.8 d (Herbig et al. 2003). Unless FU Ori is rotating much faster than the above estimates suggest, it is difficult to attribute the hard-band variability to rotational effects such as an active region rotating across the line-of-sight.

If the variability is due to a magnetic reconnection flare (e.g. in the corona) then a rough upper limit on the size of the flaring region L can be obtained using the relation $L < V_A \tau_{rise} \sim V_s \tau_{rise}$, where V_A and V_s are the Alfvén speed and sound speed respectively. Assuming a solar abundance plasma and adiabatic constant $\gamma = 5/3$, then $V_s = 1.67 \sqrt{kT/m_p}$ where m_p is the proton mass. Using $kT = 2.2$ keV from the *Chandra* spectral fit during the first half of the observation before flare peak we obtain $V_s = 8 \times 10^7$ cm s $^{-1}$ and thus $L < 4 \times 10^{12}$ cm ($L < 58 R_\odot$).

Estimates of the flare loop length based on the light curve decay timescale $\tau_{decay} \sim 23$ ks and RTV scaling laws (eq. [14] of Serio et al. 1991) give values $L_{loop} \sim (5 - 7) \times 10^{11}$ cm ($L_{loop} \sim 7 - 10 R_\odot$), consistent with the above upper limit. This value of L_{loop} is comparable to the inner radius $R_{in} \sim 5 R_\odot$ of FU Ori’s accretion disk (Malbet et al. 2005; Quanz et al. 2006; Zhu et al. 2007), raising the interesting possibility that the flare occurred in the star-disk interconnection region. However, the above calculation assumes a single loop whereas the actual physical picture is likely to be much more complicated, involving multiple loops and arcades. Also, the light curve decay timescale does not necessarily reflect the thermodynamic decay timescale since energy input may occur during the decay phase. Thus, the computed value of L_{loop} can only be considered an order-of-magnitude estimate of the length scale and does not necessarily correspond to the length of any particular loop or arcade structure on the star.

4.3. X-ray Absorption

The visual extinction toward FU Ori is estimated to be $A_V = 1.5 - 2.4$ mag (Herbig 1977; Adams et al. 1987; Kenyon et al. 1988; Green et al. 2006; Zhu et al. 2007; Kravtsova et al. 2008). This equates to an equivalent neutral H absorption column density $N_H = (3.3 - 5.3) \times 10^{21}$ cm $^{-2}$ using the Gorenstein (1975) conversion, or $N_H = (2.4 - 3.8) \times 10^{21}$ cm $^{-2}$ using the Vuong et al. (2003) conversion. These N_H values are clearly not consistent with the much larger values inferred for the hottest plasma component in the spectral models (Table 3), which we now know originates almost entirely in FU Ori. Thus, we are undoubtedly detecting excess X-ray absorption toward FU Ori, a strong indication of an anomalously large gas-to-dust ratio.

A detailed discussion of X-ray absorption based on *XMM-Newton* spectra of FU Ori was given by S06. That discussion largely carries over to the present *Chandra* analysis, but with one simplification. Specifically, S06 argued that inhomogeneous absorption due to a partially obscured corona in FU Ori was a possible means of explaining the different absorption values of the cool and hot components. This interpretation now seems overly complicated given

that *Chandra* shows the soft-band emission peak to be offset from FU Ori. A more natural explanation is that the cool low-absorption emission originates partially in the companion, which is viewed through lower X-ray absorption

There is no shortage of candidates to explain the high X-ray absorption toward FU Ori. These include dense gas in the disk or accretion stream, or FU Ori’s cool wind (or some combination thereof). Hydrodynamical simulations predict that for FUors in the rapid-accretion outburst stage the disk should be geometrically thick and the star will be enveloped by opaque disk gas (Kley & Lin 1996). It has also been suggested that FU Ori’s disk may have puffed up inner walls (Fig. 6 of Kravtsova et al. 2007) which could increase obscuration of the central star. But, there is not universal agreement on the structure of FU Ori’s disk. Malbet et al. (2005) have shown that relatively simple flat optically thick disk models can satisfactorily reproduce their VLTI data. Given our imprecise knowledge of FU Ori’s inner disk structure and the relative large disk inclination angle $i \approx 55^\circ$, FU Ori’s cool wind remains a strong candidate for explaining the high X-ray absorption. Indeed, X-ray absorption by the wind is very difficult to avoid.

It was shown by S06 that absorption by the wind alone would produce a column density $N_{\text{H,wind}} \sim 10^{24} \text{ cm}^{-2}$. This estimate was based on canonical wind parameters for FU Ori ($\dot{M} \sim 10^{-5} M_\odot \text{ yr}^{-1}$, $v_\infty = 400 \text{ km s}^{-1}$), and assumes an ideal spherically-symmetric, homogenous wind. The above value is an order of magnitude larger than inferred for the hard X-ray component of FU Ori. The two values could be brought into agreement if FU Ori’s mass-loss rate were an order of magnitude smaller: $\dot{M} \sim 10^{-6} M_\odot \text{ yr}^{-1}$. This smaller value is plausible, given that the mass-loss rate determined from analysis of optical line profiles (e.g. Croswell et al. 1987) is sensitive to several poorly-known stellar and wind parameters (S06).

The wind opacity to X-rays decreases toward higher energies, so wind absorption will be greatest at lower energies. Assuming an ideal solar-abundance wind, canonical FU Ori wind parameters (Croswell et al. 1987), and photoelectric absorption cross-sections from Balucińska-Church & McCammon (1992), the radius of optical depth unity is $R_{\tau=1} \approx 10 \text{ AU}$ at $E = 1 \text{ keV}$ and $R_{\tau=1} \approx 1 - 2 \text{ AU}$ at $E = 2 \text{ keV}$. Thus, the wind is capable of absorbing very soft X-rays that might arise in an accretion shock at the stellar surface. On the other hand, hard X-rays at $E \gtrsim 2 - 3 \text{ keV}$ can escape through the wind.

4.4. X-ray Luminosity

Chandra spectral fits give an unabsorbed X-ray luminosity for FU Ori of $\log L_X(0.3 - 8 \text{ keV}) = 30.76 - 31.09 \text{ ergs s}^{-1}$ at an assumed distance of 460 pc (Table 3). This is the

time-averaged value based on the full exposure. Because of the hard-band flare (Fig. 3), L_X varied by at least $\approx 60\%$ between the first half and second half of the observation. A small fraction of the total X-ray luminosity ($\lesssim 12\%$) is attributable to the companion. *XMM-Newton* yielded similar L_X values (S06). The L_X value for FU Ori is quite high for a young low-mass star, and is near the maximum observed for accreting TTS in the Orion COUP survey (Fig. 17 of Preibisch et al. 2005). A similarly high L_X was found for V1735 Cyg, the other FUor detected in our *XMM-Newton* survey (Skinner et al. 2009).

The high X-ray luminosity of FU Ori is even more remarkable if the mass of the central star is $M_* \approx 0.3 M_\odot$, as inferred from radiative transfer disk models by Zhu et al. (2007). Previous X-ray studies have shown that L_X is correlated with M_* in TTS, albeit with rather large scatter (Feigelson et al. 1993; Preibisch et al. 2005; Telleschi et al. 2007). The parameters obtained for linear regression fits depend somewhat on the choice of evolutionary tracks used to determine stellar masses, and on the sample of TTS being analyzed. For a star of $0.3 M_\odot$, the $L_X \propto M_*$ correlation based on the Orion COUP results (Preibisch et al. 2005) predicts $\log L_X = 29.75 \text{ ergs s}^{-1}$, with a standard deviation of 0.64 dex. The correlation obtained for cTTS in the *XMM-Newton* survey of Taurus (Telleschi et al. 2007) predicts $\log L_X = 29.24 (\pm 0.19) \text{ ergs s}^{-1}$. These predictions are an order of magnitude below that observed for FU Ori.

If FU Ori is indeed a subsolar mass star, then its X-ray luminosity is significantly higher than expected based on the above comparisons with TTS. The reason for the excess is not yet clear, but several factors could play a role. These include rapid rotation (Herbig et al. 2003), a putative spectroscopic companion (Malbet et al. 2005; Vittone & Errico 2005; Reipurth & Aspin 2004), or an additional X-ray contribution from the magnetized accretion disk or disk corona.

Another possibility is that FU Ori is an intermediate mass star. If the $L_X \propto M_*$ relation for TTS applies to FUors (not yet proven), then the inferred mass of FU Ori is $M_* \sim 2 M_\odot$. Interestingly, Herbig et al. (2003) have suggested that FU Ori might have a substantial mass $(M_*/M_\odot)\sin i > 0.79$, where i is the inclination of the star’s rotation axis.

4.5. Comparison with T Tauri Stars

FU Ori is not the only accreting young star for which multiple X-ray absorption components are required to obtain acceptable spectral fits. Other recent examples are the classical T Tauri stars DG Tau, GV Tau, and DP Tau (Güdel et al. 2007; 2008; 2009). These three stars show strikingly similar X-ray properties to FU Ori, namely: (i) a lightly-absorbed non-

variable soft component, and (ii) a variable hard component whose absorption is about an order-of-magnitude greater than expected from visual extinction estimates. However, these three accreting TTS differ from FU Ori in the respect that they are all known to drive *optical* jets. Similarly, the young binary system Z CMa is known to drive an optical jet and soft X-ray emission displaced $\approx 2''$ along its optical jet axis was reported by Stelzer et al. (2009). In contrast, there is so far no confirmed evidence for a well-delineated bipolar optical or X-ray jet in FU Ori. But, as we have noted (Sec. 4.1), there is a pending report of a HH object a few arcseconds northeast of FU Ori so further high-resolution searches for a collimated jet near the star are warranted.

Analysis of the X-ray data for the above three cTTS led Güdel et al. (2007) to the conclusion that their hard variable emission was due to an active corona, which is also a reasonable explanation for FU Ori. The strong X-ray absorption was attributed to mass inflow from the accretion disk. Accreting gas is also a possible explanation for FU Ori’s high X-ray absorption, but its strong cool wind seems to be a more straightforward explanation.

Güdel et al. (2007) also concluded that the soft X-ray emission component in the sample of jet-driving cTTS was not cospatial with the hard emission. This was immediately apparent in DG Tau images, which showed soft X-ray emission extending outward $\approx 5''$ from the star along the optical jet axis (Güdel et al. 2008). Further analysis of the DG Tau *Chandra* images showed that the soft-band X-ray centroid position was offset by $0.''2$ from the hard-band centroid in the general direction of the optical jet (Schneider & Schmitt 2008). The soft emission from the jet thus apparently extends inward to within a distance of ~ 48 AU from the star. The soft extended X-rays are thought to be produced by shocks or magnetic heating in the DG Tau jet (Güdel et al. 2008).

Similarly, we have demonstrated here that the soft X-ray emission in FU Ori is not cospatial with the hard emission. The magnitude of the soft-band centroid offset is comparable to that found for DG Tau (Schneider & Schmitt 2008). However, unlike the case for DG Tau, the displacement of the soft emission to the southeast of FU Ori does not obviously coincide with a jet, since there is no supporting evidence for an optical jet or collimated outflow directed to the southeast. Instead, the offset of the soft emission is toward FU Ori’s companion. Either the companion is an X-ray source (which we believe is likely), or soft X-rays are somehow produced *in situ* between the two stars (e.g. via wind shocks, as discussed with caveats in Sec. 4.1). In either case, FU Ori’s companion seems to play a direct or indirect role in producing the detected soft X-ray emission. This raises the interesting question of what role, if any, close companions might play in producing the soft X-ray emission of jet-driving TTS. In the case of DG Tau, which provides the most dramatic example to date of a TTS with a clearly-delineated optical and X-ray jet, searches for a companion have so

far yielded negative results (Leinert et al. 1991).

5. Summary

The new *Chandra* X-ray data for FU Ori analyzed here both clarify and extend earlier results based on a shorter *XMM-Newton* exposure. *Chandra* has revealed that the cool and hot X-ray components are spatially distinct. The hot heavily-absorbed component originates almost entirely in FU Ori and accounts for most of the intrinsic X-ray luminosity. The hot component is variable and is likely coronal emission originating close to the star and viewed through heavy absorption from FU Ori’s wind or accreting gas. The presence of X-ray variability in young stars is usually attributed to magnetic fields. Thus, the new *Chandra* data substantiate the previous report of a magnetic field (Donati et al. 2005).

The cool moderately-absorbed X-ray component accounts for the emission below 2 keV and has so far not shown variability. The 0."2 southeastward offset of the soft-band emission toward the near-IR companion (FU Ori S) is strong evidence that the companion contributes significantly to the detected emission below 2 keV. The companion also appears to contribute weakly to the emission above 2 keV. The combination of a cool and hot component from the companion is not unexpected if it is a young K-type star (e.g. a TTS), since TTS in the Orion COUP survey generally show such multi-temperature plasma that in most cases is thought to be of coronal origin (Preibisch et al. 2005). As a result of the offset, the soft emission is seen through a much lower absorption column density than toward FU Ori itself. This explains why fits of *XMM-Newton* spectra obtained at lower angular resolution required two unequal absorption components from an apparently single X-ray source.

The *Chandra* observation discussed here provides the most detailed picture of FU Ori’s X-ray emission so far, but further long-term X-ray monitoring would be useful. Such monitoring could determine if FU Ori’s hard-band X-ray variability is periodic, and if so whether the period agrees with previously surmised rotation rates of 8.76 d (Popham et al. 1996) or 14.8 d (Herbig et al. 2003).

Periodic variability might also be present on longer timescales if there is a third component in the system orbiting very close to FU Ori. A third component in a close eccentric orbit was cited by Malbet et al. (2005) as one possible means of explaining a low-amplitude oscillation seen in their VLTI long-baseline data. A low-mass companion orbiting in FU Ori’s disk was also cited as a possible cause of periodic H α emission line variations in FU Ori (Vittone & Errico 2005). And, Reipurth & Aspin (2004) have proposed a scenario which predicts that FU Ori is a close (<10 AU) binary. The presence of a low-mass object such as a

protoplanet, brown dwarf, or very low-mass star in a close eccentric orbit within a few AU of FU Ori could induce X-ray variability. This has been demonstrated in recent *XMM-Newton* observations of HD 189733, which detected changes in the X-ray spectrum and a flare during the eclipse and transit of its hot-Jupiter planet (Pillitteri et al. 2010).

This work was supported by *Chandra* award GO9-0005X issued by the Chandra X-ray Observatory Center (CXC). The CXC is operated by the Smithsonian Astrophysical Observatory (SAO) for, and on behalf of, the National Aeronautics Space Administration under contract NAS8-03060. We thank P. Garcia and C. Dougados for information on the location of the Herbig-Haro object near FU Ori prior to publication.

REFERENCES

- Adams, F.C., Lada, C.J., & Shu, F.H., 1987, *ApJ*, 312, 788
- Anders, E., & Grevesse, N. 1989, *Geochim. Cosmochim. Acta*, 53, 197
- Bally, J., Feigelson, E., & Reipurth, B. 2003, *ApJ*, 584, 843
- Balucińska-Church, M. & McCammon, D. 1992, *ApJ*, 400, 699
- Calvet, N., Hartmann, L., & Kenyon, S.J., 1993, *ApJ*, 402, 623
- Croswell, K., Hartmann, L., & Avrett, E.H., 1987, *ApJ*, 312, 227
- Donati, J.-F., Paletou, F., Bouvier, J., & Ferreira, J. 2005, *Nature*, 438, 466
- Errico, L., Vittone, A., & Lamzin, S.A. 2003, *Ast. Lett.*, 29, 105
- Feigelson, E.D., Casanova, S., Montmerle, T., & Guibert, J. 1993, *ApJ*, 416, 623
- Gorenstein, P., 1975, *ApJ*, 198, 95
- Green, J.D. et al. 2006, *ApJ*, 648, 1099
- Gregory, P.C., & Lored, T.J., 1992, *ApJ*, 398, 146
- Gregory, P.C., & Lored, T.J., 1996, *ApJ*, 473, 1059
- Güdel, M., Skinner, S.L., Briggs, K.R., Audard, M., Arzner, K., & Telleschi, A., 2005, *ApJ*, 626, L53

- Güdel, M., Skinner, S.L., Audard, M., Briggs, K., & Cabrit, S. 2008, *A&A*, 478, 797
- Güdel, M., Telleschi, A., Audard, M., Skinner, S.L., Briggs, K.R., Palla, F., & Dougados, C. 2007, *A&A*, 468, 515
- Güdel, M. et al. 2009, in *Protostellar Jets in Context*, eds. K. Tsinganos, T. Ray, & M. Stute (Berlin: Springer), 347
- Hartigan, P., Edwards, S., & Ghandour, L. 1995, *ApJ*, 452, 736
- Hartmann, L. & Kenyon, S.J. 1996, *ARA&A*, 34, 207 (HK96)
- Herbig, G.H. 1966, *Vistas in Astron.*, 8, 109
- Herbig, G.H. 1977, *ApJ*, 217, 693
- Herbig, G.H., Petrov, P.P., & Duemmler, R., 2003, *ApJ*, 595, 384
- Kenyon, S.J., Hartmann, L., & Hewett, R., 1988, *ApJ*, 325, 231
- Kley, W. & Lin, D.N.C. 1996, *ApJ*, 461, 933
- Kravtsova, A.S., Lamzin, S.A., Errico, L., & Vittone, A. 2007, *Ast. Letters*, 33, 755
- Kravtsova, A.S., Malogolovets, E.V., & Lamzin, S.A. 2008, *Astrophys. Bull.*, 63, 357
- Leinert, Ch., Haas, M., Mundt, R., Richichi, A., & Zinnecker, H. 1991, *A&A*, 250, 407
- Levreault, R.M., 1988, *ApJ*, 330, 897
- Malbet, F. et al. 2005, *A&A*, 437, 627
- Petrov, P.P. & Herbig, G.H., 1992, *ApJ*, 392, 209
- Pillitteri, I., Wolk, S.J., Cohen, O., Kashyap, V., Knutson, H., & Lisse, C.M. 2010, *BAAS*, 41, 685
- Popham, R., Kenyon, S., Hartmann, L., & Narayan, R. 1996, *ApJ*, 473, 422
- Preibisch, T. et al. 2005, *ApJS*, 160, 401
- Press, W.H., Teukolsky, S.A., Vetterling, W.T., & Flannery, B.P., 1992, *Numerical Recipes in Fortran: The Art of Scientific Computing* (2nd ed.; New York: Cambridge Univ. Press), 617
- Quanz, S.P., Henning, Th., Bouwman, J., Ratzka, Th., & Leinert, Ch., 2006, *ApJ*, 648, 472

- Raga, A.C., Noriega-Crespo, A., & Velázquez, P.F., 2002, ApJ, 576, L149
- Reipurth, B. & Aspin, C. 2004, ApJ, 608, L65
- Reipurth, B. & Aspin, C. 2010, to appear in *Evolution of Cosmic Objects Through Their Physical Activity*, eds. H. Harutyunyan, A. Mickaelian, & Y. Terzian (Yerevan: Gitutyun Publishing House), in press
- Rodriguez, L.F., Hartmann, L.W., & Chavira, E., 1990, PASP, 102, 1413
- Sandell, G. & Weintraub, D.A. 2001, ApJS, 134, 115
- Schneider, P.C. & Schmitt, J.H.M.M. 2008, A&A, 488, L13
- Serio, S., Reale, F., Jakimiec, J., Sylwester, B., & Sylwester, J. 1991, A&A, 241, 197
- Skinner, S.L., Briggs, K.R., & Güdel, M. 2006, ApJ, 643, 995 (S06)
- Skinner, S.L., Sokal, K.R., Güdel, M., & Briggs, K.R. 2009, ApJ, 696, 766
- Smith, H.A., Thronson, H.A., Lada, C.J., Harper, D.A., Loewenstein, R.F., & Smith, J., 1982, ApJ, 258, 170
- Stelzer, B., Hubrig, S., Orlando, S., Micela, G., Mikulášek, Z., & Schöller, M. 2009, A&A, 499, 529
- Stevens, I.R., Blondin, J.M., & Pollock, A.M.T. 1992, ApJ, 386, 265
- Telleschi, A., Güdel, M., Briggs, K.R., Audard, M., & Palla, F. 2007, A&A, 468, 425
- Vittone, A.A. & Errico, L., 2005, Mem. S.A. It., 76, 320
- Vuong, M.H., Montmerle, T., Grosso, N., Feigelson, E.D., Verstraete, L., & Ozawa, H. 2003, A&A, 408, 581
- Wang, H., Apai, D., Henning, T., & Pascucci, I., 2004, ApJ, 601, L83
- Zhu, Z., Hartmann, L., Calvet, N., Hernandez, J., Muzerolle, J., & Tannirkulam, A.-K. 2007, ApJ, 669, 483

Table 1. X-ray Properties of FU Ori (Chandra ACIS-S)

Name	R.A. (J2000)	Decl. (J2000)	Net Counts (cts)	E ₅₀ (keV)	\bar{E} (keV)	P _{var} KS	P _{var} GL	Identification(offset) (arcsec)
FU Ori	05 45 22.361	+09 04 12.33	296±17	3.64	3.60	0.999	0.934	2MASS J054522.357+090412.40 (0.09)

Note. — X-ray data are from CCD7 (ACIS chip S3) using events in the 0.3 - 8 keV range inside a 3σ source extraction ellipse with semi-major and semi-minor axes of 1.''31 and 1.''19 respectively. Tabulated quantities are: J2000.0 X-ray position (R.A., Decl.), corrected for systematic offsets (Sec. 3.1); net counts and net counts error from *wavdetect* (accumulated in a 98867 s exposure, rounded to the nearest integer, background subtracted and PSF-corrected); median photon energy (E₅₀), mean photon energy (\bar{E}); probability of variable count-rate determined by the Kolmogorov-Smirnov (KS) test and the Gregory-Loredo (GL) algorithm (P_{var}); and 2MASS counterpart identification. The offset (in parenthesis) is given in arc seconds between the X-ray and 2MASS counterpart position.

Table 2. FU Ori X-ray Centroid Positions (Chandra ACIS-S)

Band	R.A. (h m s \pm s)	Decl. ($^{\circ}$ ' " \pm ")	Δ R.A. (s)	Δ Decl. (")
Broad (0.3 - 8 keV)	05 45 22.361 \pm 0.001	+09 04 12.33 \pm 0.02	+0.004	–0.07
Hard (2 - 8 keV)	05 45 22.359 \pm 0.001	+09 04 12.37 \pm 0.02	+0.002	–0.03
Soft (0.3 - 2 keV)	05 45 22.363 \pm 0.001	+09 04 12.22 \pm 0.05	+0.006	–0.18

Note. — X-ray centroid positions (J2000.0) are from XIMAGE and have been corrected for small systematic offsets based on registration against 2MASS near-IR sources (Sec. 3.1). The positions were measured from subpixel images with pixel randomization removed. The offsets Δ R.A. and Δ Decl. are relative to the 2MASS position of FU Ori (J054522.357+090412.40) and are in the sense of CXO – 2MASS. The quoted uncertainties reflect only the range of values determined by the different centroiding algorithms. Statistical uncertainties are larger and their determination would need to take into account numerous factors such as the uncertainties in the near-IR positions of the 2MASS sources used for cross-registration.

Table 3. *Chandra* Spectral Fits for FU Ori

Parameter			
Model ^a	A	B	C
Emission	Thermal (2T)	Thermal (3T)	Thermal (3T)
Abundances	solar ^b	solar	solar ^c
N _{H,1} (10 ²² cm ⁻²)	0.97 [0.70 - 1.51]	0.34 [0.13 - 1.35]	0.41 [0.00 - 0.83]
N _{H,2} (10 ²² cm ⁻²)	9.20 [5.95 - 16.3]	12.2 [7.75 - 19.8]	2.40 [1.05 - 7.60]
N _{H,3} (10 ²² cm ⁻²)	12.0 [7.44 - 19.6]
kT ₁ (keV)	0.53 [0.36 - 0.74]	0.19 [0.00 - 0.45]	0.20 [0.06 - 0.50]
kT ₂ (keV)	4.50 [1.85 - 12.2]	{3.0}	0.39 [0.11 -]
kT ₃ (keV)	...	2.99 [1.58 - 9.17]	2.92 [1.44 - 8.34]
norm ₁ (10 ⁻⁶) ^d	8.65 [0.98 -]	5.05 [0.03 - ...]	8.60 [0.30 -]
norm ₂ (10 ⁻⁴) ^d	1.16 [0.60 - 4.90]	0.036 [0.02 - 0.13]	0.72 [0.20 - 2.30]
norm ₃ (10 ⁻⁴) ^d	...	1.90 [0.78 - 4.37]	2.00 [0.80 - 8.10]
χ ² /dof	27.8/23	16.8/22	15.2/20
χ ² _{red}	1.21	0.76	0.76
F _X (10 ⁻¹⁴ ergs cm ⁻² s ⁻¹)	5.83 (22.5)	5.74 (31.5)	5.73 (48.5)
F _{X,1} (10 ⁻¹⁴ ergs cm ⁻² s ⁻¹)	0.18 (2.22)	0.46 (1.40)	0.11 (1.49)
F _{X,2} (10 ⁻¹⁴ ergs cm ⁻² s ⁻¹)	5.65 (20.3)	5.28 (30.1)	0.16 (15.2)
F _{X,3} (10 ⁻¹⁴ ergs cm ⁻² s ⁻¹)	5.46 (31.6)
log L _X (ergs s ⁻¹)	30.76	30.90	31.09
log [L _X /L _{bol}]	-5.37	-5.23	-5.04

Note. — Based on XSPEC (vers. 12.4.0) fits of the background-subtracted ACIS-S spectrum binned to a minimum of 10 counts per bin using 98,867 sec of exposure time. Thermal emission was modeled with the *apec* and *vaptec* optically thin plasma models in XSPEC. The tabulated parameters are absorption column density (N_H), plasma energy (kT), and XSPEC component normalization (norm). Solar abundances are referenced to Anders & Grevesse (1989). Square brackets enclose 90% confidence intervals and an ellipsis means that the algorithm used to compute confidence intervals did not converge. Quantities enclosed in curly braces were held fixed during fitting. The total X-ray flux (F_X) and fluxes associated with each model component (F_{X,i}) are the absorbed values in the 0.3 - 8 keV range, followed in parentheses by unabsorbed values. The total X-ray luminosity L_X is the unabsorbed value in the 0.3 - 8 keV range and assumes a distance of 460 pc. A value L_{bol} = 350 L_⊙ is adopted based on an average of values given in the literature (HK96, Levreault 1988, Sandell & Weintraub 2001, Smith et al. 1982).

^aModel A: N_{H,1}·kT₁ + N_{H,2}·kT₂;

Model B: N_{H,1}·(kT₁ + kT₂) + N_{H,2}·kT₃

Model C: N_{H,1}·kT₁ + N_{H,2}·kT₂ + N_{H,3}·kT₃.

^bVarying the Fe abundance gives Fe = 0.55 [0.0 - 1.16] × solar but does not significantly improve the fit.

^cVarying the Fe abundance gives Fe = 0.63 [0.14 - 1.24] × solar but does not significantly improve the fit.

^dFor thermal *vaptec* models, the norm is related to the volume emission measure (EM = n_e²V) by EM = 4π10¹⁴d_{cm}²×norm, where d_{cm} is the stellar distance in cm. At d = 460 pc, this becomes EM = 2.53×10⁵⁷ × norm (cm⁻³).

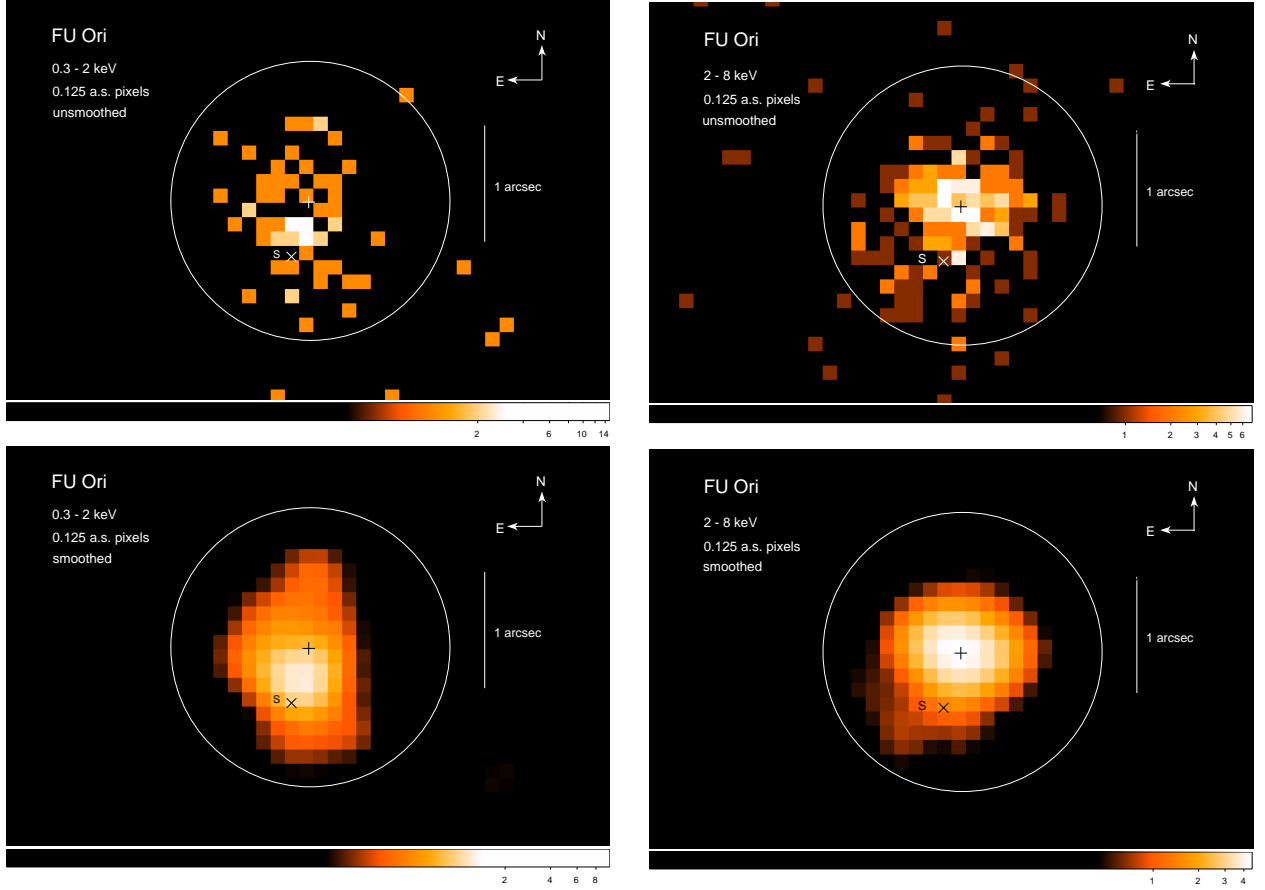


Fig. 1.— Soft-band (0.3 - 2 keV) and hard-band (2 - 8 keV) ACIS-S images of FU Ori. Pixel randomization has been removed and the images were binned to a subpixel size of $0.''125$. The + sign marks the 2MASS position of FU Ori and the x shows the position of the near-IR companion FU Ori S. The 70% encircled energy region at 3 keV is shown by the circle of radius $R_{70} = 1.''2$. The value of R_{70} is nearly independent of energy. The intensity scale is logarithmic. *Top*: Unsmoothed *Bottom*: Gaussian-smoothed

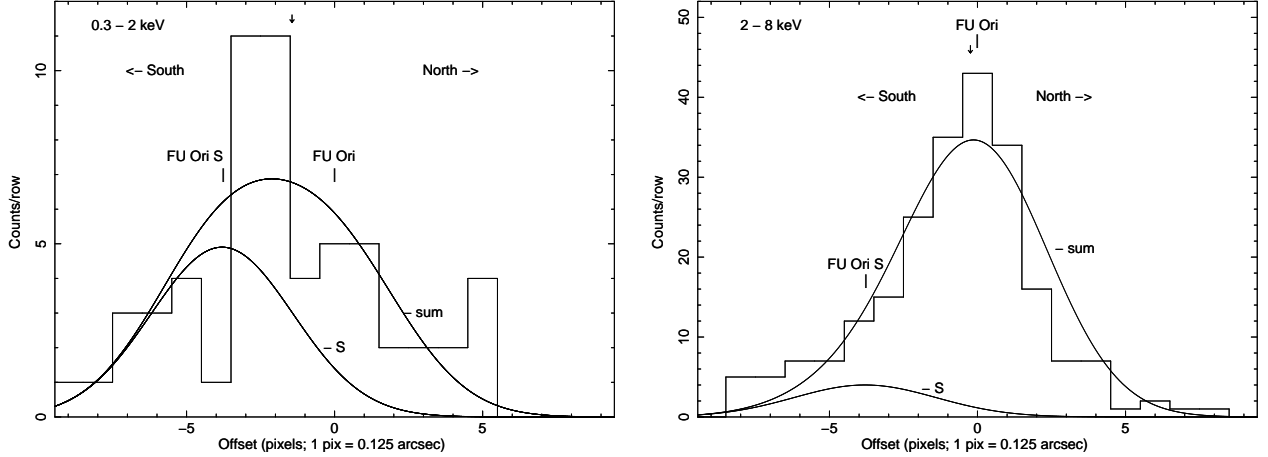


Fig. 2.— Histograms showing the number of soft-band (0.3 - 2 keV) and hard-band (2 - 8 keV) counts in each row of FU Ori sub-pixel images ($0.''125$ pixels) measured within the 70% EEf circle of radius $R_{70} = 1.''2$ (see Fig. 1). Within this circle there are 59 soft-band and 223 hard-band counts. Each row represents a horizontal slice of one-pixel breadth through the image in the EW direction. The row passing through the FU Ori 2MASS position corresponds to offset = 0. Rows lying north of FU Ori have positive offsets. The companion FU Ori S lies south of FU Ori at a projected NS separation of $0.''47$ (Offset = -3.8 pixels). Downward arrows mark the centroid positions determined from analysis of 2D images with XIMAGE. The soft-band centroid is offset $0.''18$ (-1.44 pixels) south of FU Ori, toward the companion. The soft-band peak lies slightly south of the centroid, at an offset of $0.''31$ (-2.5 pixels). The hard-band peak is coincident with FU Ori but the hard-band centroid is slightly offset to the south by $0.''03$ (-0.24 pix). The large Gaussian curve in each panel shows the two-component fit obtained by summing two Gaussians. One Gaussian was centered at the FU Ori position (offset = 0.0) and other at FU Ori S (offset = -3.8). The Gaussian widths were fixed at FWHM = 2.5 pixels ($0.''74$), corresponding to the ACIS-S PSF core FWHM at 1.5 keV. The PSF core FWHM increases slightly with energy, but the dependence is weak and is ignored here. The small Gaussian curve in each panel shows the contribution to the total fit from FU Ori S. In the soft-band, the Gaussian fit attributes 28 [14 - 40; 90% conf.] counts to FU Ori and 31 [16 - 42] counts to the companion. In the hard-band, the respective contributions are 196 [173 - 219] counts from FU Ori and 27 [4 - 48] counts from the companion.

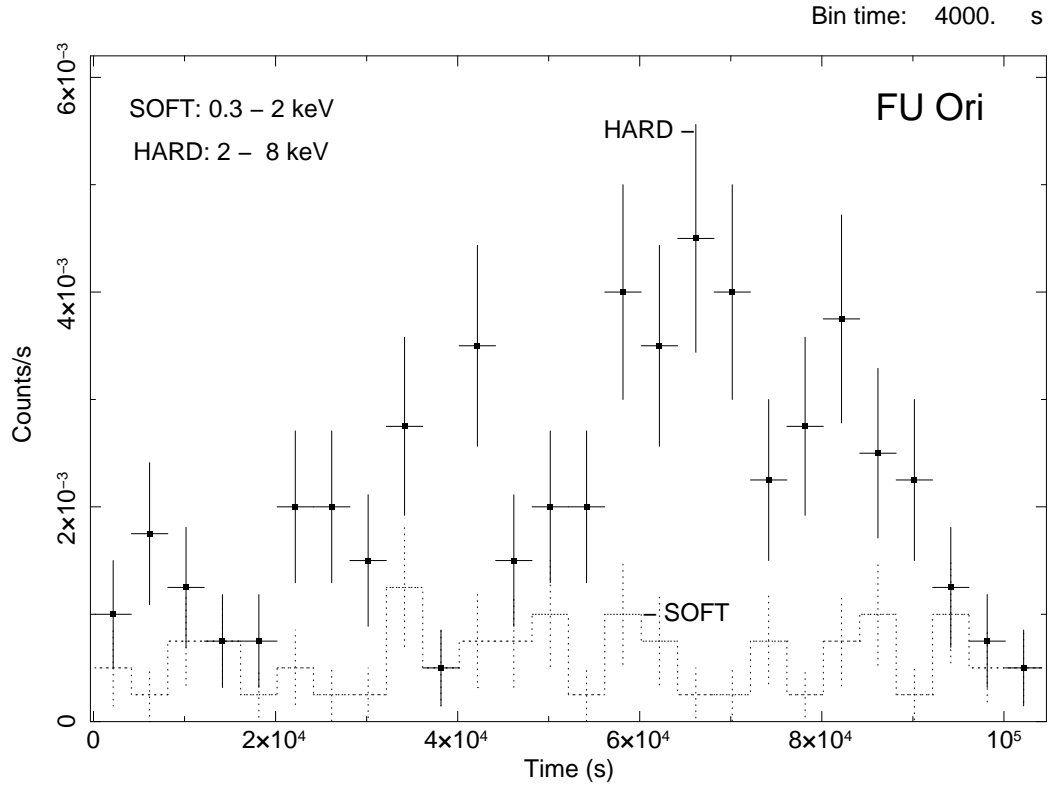


Fig. 3.— Chandra ACIS-S light curves of FU Ori in soft (0.3 - 2 keV; dotted line) and hard (2 - 8 keV) energy bands. The binsize is 4000 s. Error bars are 1σ .

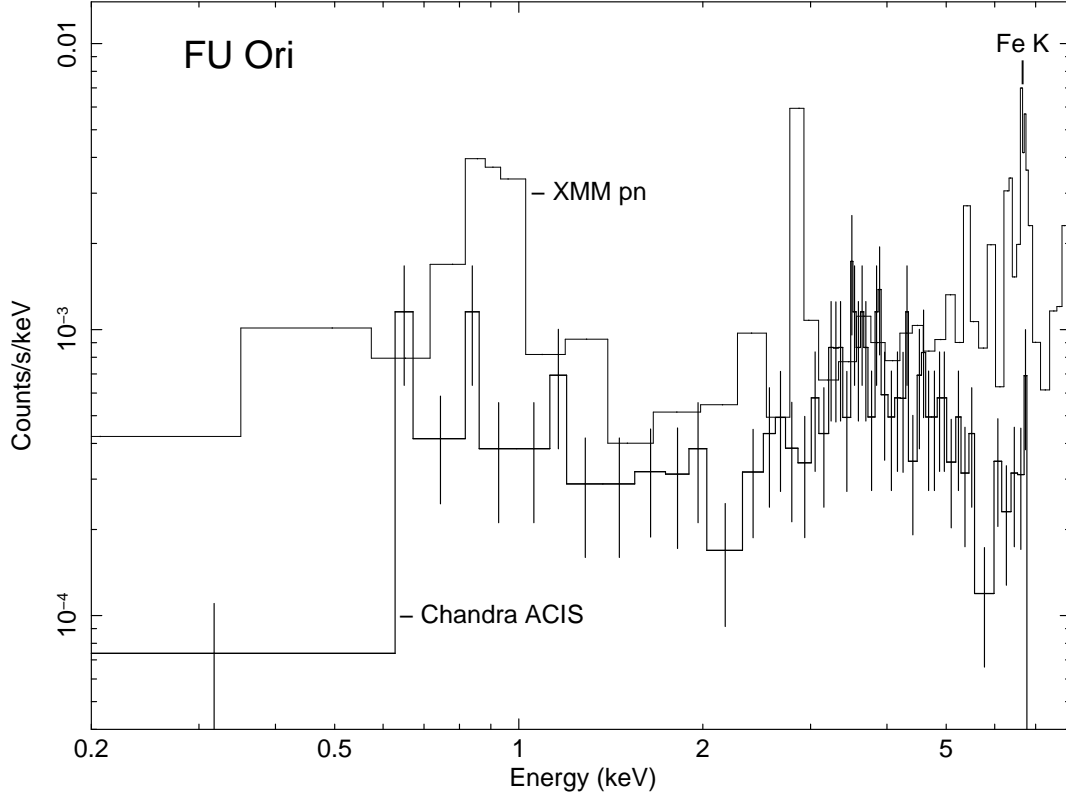


Fig. 4.— Chandra ACIS-S and XMM EPIC pn spectra of FU Ori. Both spectra are binned to a minimum of 5 counts per bin. The ACIS-S spectrum is based on an exposure livetime of 98,867 s (background is negligible) and the EPIC pn spectrum is based on 26,891 s of low-background exposure. Error bars on the XMM spectrum have been removed for clarity. The solid lines are histograms and not fitted models. The Fe $K\alpha$ line complex (Fe XXV; $E = 6.67$ keV) forms at high temperatures $T \sim 40$ MK and is visible in both spectra.

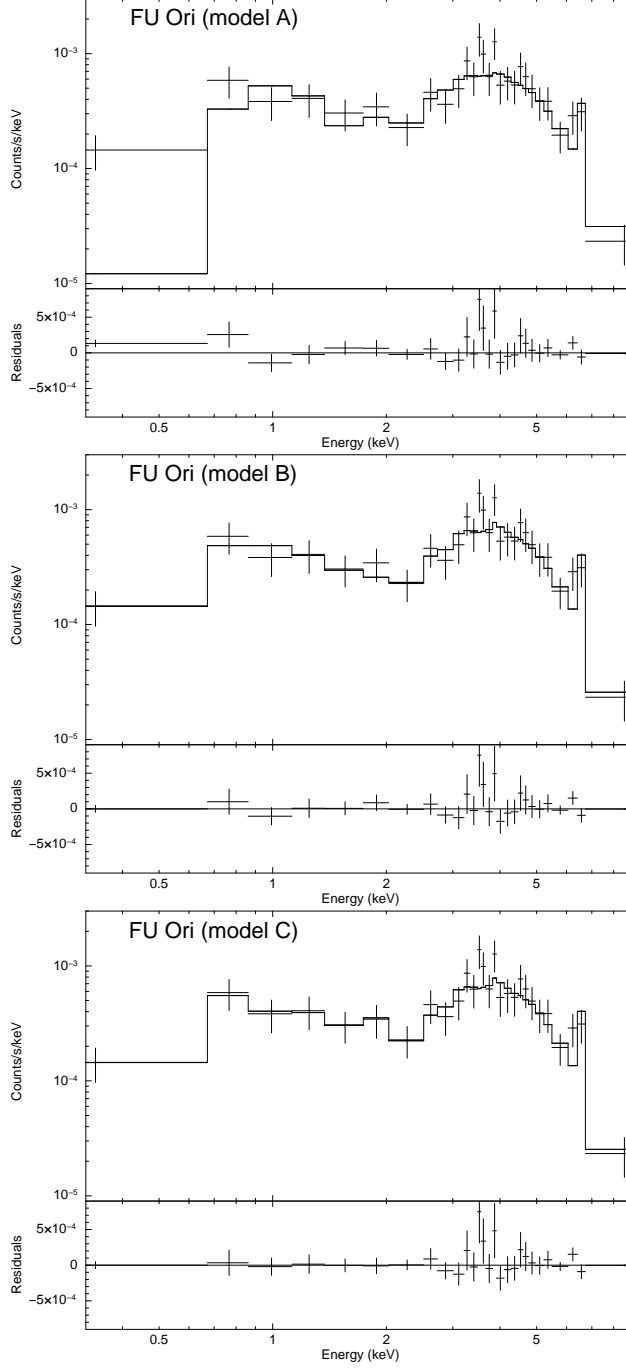


Fig. 5.— Spectral fits of the Chandra ACIS-S spectrum of FU Ori using the models summarized in Table 3. The fit below 2 keV is improved using models B and C.

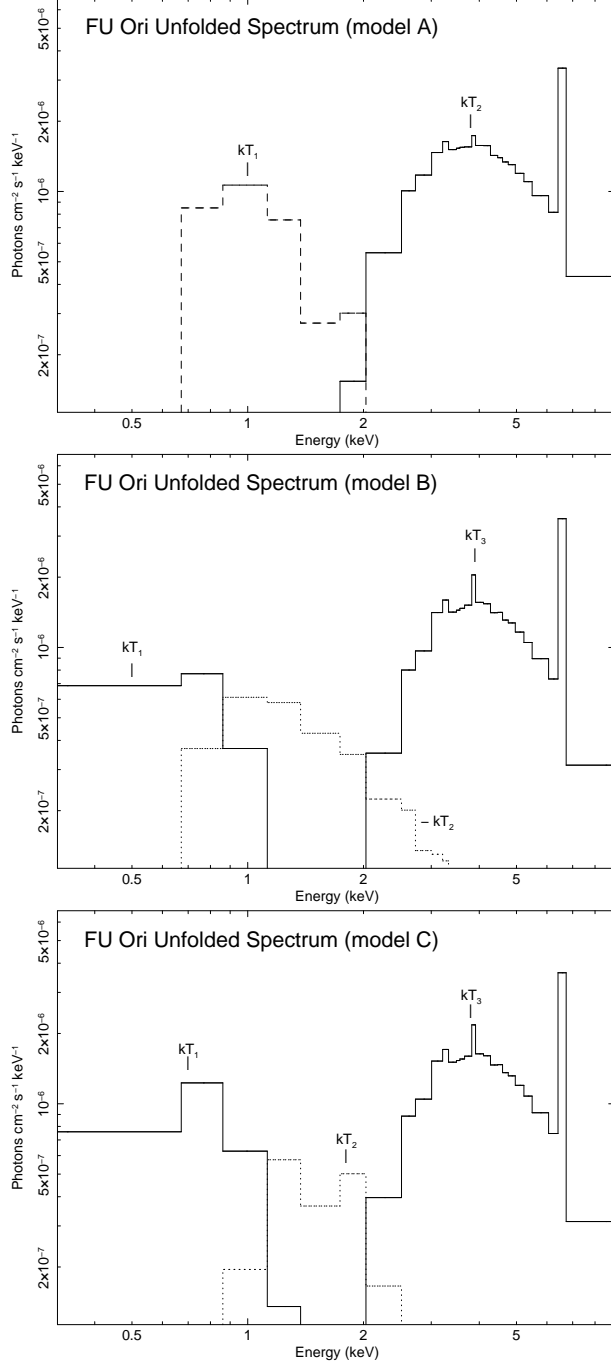


Fig. 6.— Unfolded spectra for the model fits shown in Figure 5. The hot component accounts for essentially all of the emission above 2 keV.